Electronic supplementary information

Photoinduced Intramolecular Energy Transfer and Anion Sensing Studies of Isomeric $Ru^{II}Os^{II}$ Complexes Derived from an Asymmetric Phenanthroline-Terpyridine Bridge

Dinesh Maity, Chanchal Bhaumik, Debiprasad Mondal and Sujoy Baitalik*

Department of Chemistry, Inorganic Chemistry Section, Jadavpur University, Kolkata – 700032, India

Table S1 Photophysical data of **1-3** in different solvents

Solvents	Compounds	Absorption λ_{max}/ nm (ε / $M^{-1}cm^{-1}$)	Luminescence			E^{0-0} / (eV)
			λ_{max} / nm	Φ / 10^{-3}	τ / ns	
CH_2Cl_2	**1**	461(12920), 428(sh)(10470)	600	497	426	2.31
	2	650(br)(4190), 486(20590), 438(sh)(19700)	707	237	92.06	1.87
	3	501(19750), 406(11080)	647	34.92	1.12, 30.09	2.22
CH_3OH	**1**	459(19290), 424(sh)(14760)	607	432	206	2.31
	2	650(br)(5370), 484(26030), 434(sh)(23900)	717	83.08	41.01	1.86
	3	498(44830)	656	6.80	1.14, 3.00	2.20
$(CH3)_2CO$	**1**	460(20160), 424(sh)(15730)	611	408	192	2.30
	2	653(br)(4260), 487(20000), 437(sh)(18820)	720	70.79	41.54	1.85
	3	503(51160)	660	8.96	2.60, 4.80	2.17
CH_3CN	**1**	460(17240), 426(sh)(13860)	607	297	151	2.30
	2	650(br)(5600), 486(26000), 435(sh)(24000)	720	83.15	44.31	1.85
	3	500(46420)	658	6.90	1.79, 3.34	2.17
H_2O	**1**	464(17550), 428(14380)	610	579	542	2.28
	2	665(br)(3230), 487(17870), 436(sh)(17570)	723	32.57	39.20	1.85
	3	---	--	--	--	--
DMSO	**1**	464(18000), 429(sh)(14630)	620	576	353	2.26
	2	665(br)(2790), 490(13900), 438(sh)(16320)	756	22.01	43.57	1.81
	3	508(63420)	667	21.36	3.11, 14.12	2.15

Table S2 Spectroscopic and relevant photophysical data for intramolecular energy transfer in **4** and **5** in different solvents

Solvents	Compounds	Absorption λ_{max}/ nm (ε / $M^{-1}cm^{-1}$)	Luminescence λ_{max} / nm	Φ / 10^{-3}	τ / ns	$E^{0\text{-}0}$ / eV	ΔG^0 / eV
CH_2Cl_2	**4**	674(br)(4300), 495(26600), 465(sh)(25300), 429(sh)(17400)	747	216	168	1.81	-0.50
	5	665(br)(3200), 496(50200), 440(br)(25000)	710	135	71.84	1.90	-0.32
CH_3OH	**4**	672(br)(8560), 494(52540), 464(sh)(44750), 422(sh)(33390)	743	157	107	1.82	-0.49
	5	666(3980), 496(74660)	722	73.07	39.20	1.89	-0.28
$(CH3)_2CO$	**4**	672(br)(6440), 495(35000), 466(sh)(32370), 427(sh)(24580)	753	154	120	1.80	-0.50
	5	669(br)(4740), 496(74580), 438(br)(36020)	725	75.37	40.54	1.88	-0.29
CH_3CN	**4**	672(br)(8700), 494(45600), 460(sh)(37100), 424(sh)(26600)	750	164	101	1.81	-0.49
	5	658(br)(4180), 494(66560), 439(br)(32460)	722	82.26	42.52	1.88	-0.29
H_2O	**4**	671(br)(5200), 491(33600), 465(br)(30500)	749	84.73	89.79	1.87	-0.41
	5	667(br)(2100), 495(34600), 437(br)(16400)	724	31.80	31.85	1.87	---
DMSO	**4**	680(br)(7370), 508(43640), 470(br)(34240), 427(sh)(31950)	757	195	151	1.79	-0.47
	5	674(br)(3220), 507(53980), 440(sh)(29830)	762	21.93	38.16	1.80	-0.35

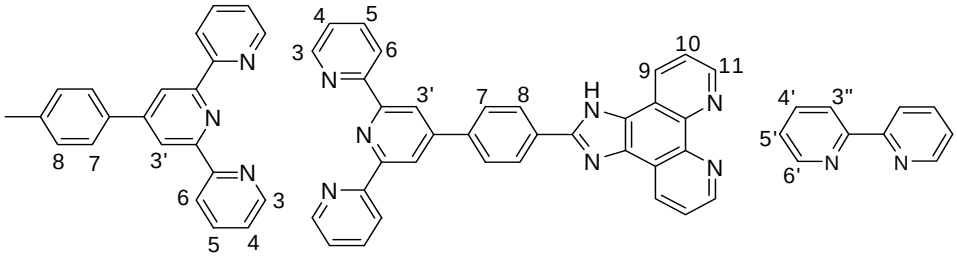

Scheme S1. Proton numbering of tpy-PhCH_3, phen-Hbzim-tpy, and bpy.

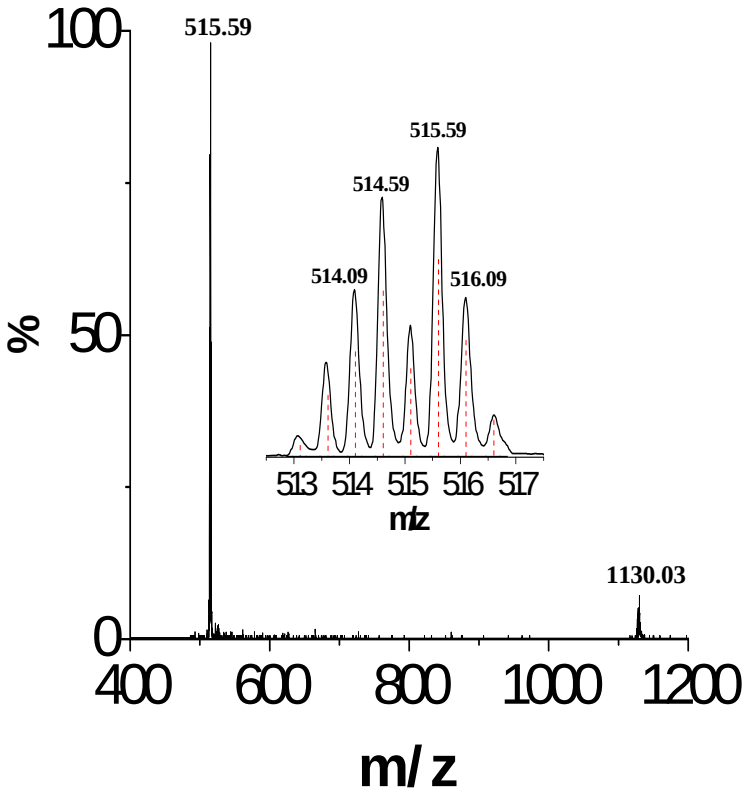

Fig. S1 ESI-MS (positive) for the complex cations $[(bpy)_2Os(phen\text{-}Hbzim\text{-}tpy)]^{2+}$ (*m/z* = 515.59) and $[(bpy)_2Os(phen\text{-}bzim\text{-}tpy)]^{+}$ (*m/z* = 1130.03) in acetonitrile showing the observed and isotopic distribution patterns.

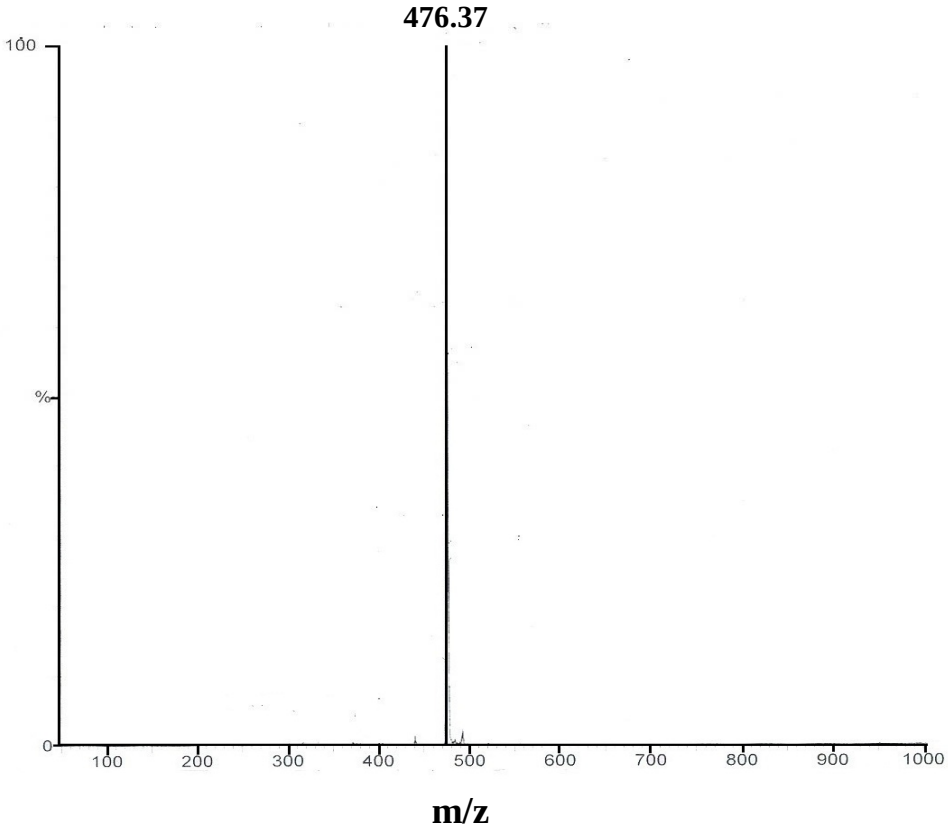

Fig. S2 ESI-MS (positive) for the complex $[(tpy–PhCH_3)Ru(tpy\text{-}Hbzim\text{-}phen)]^{2+}$ (*m/z* = 476.37) in acetonitrile.

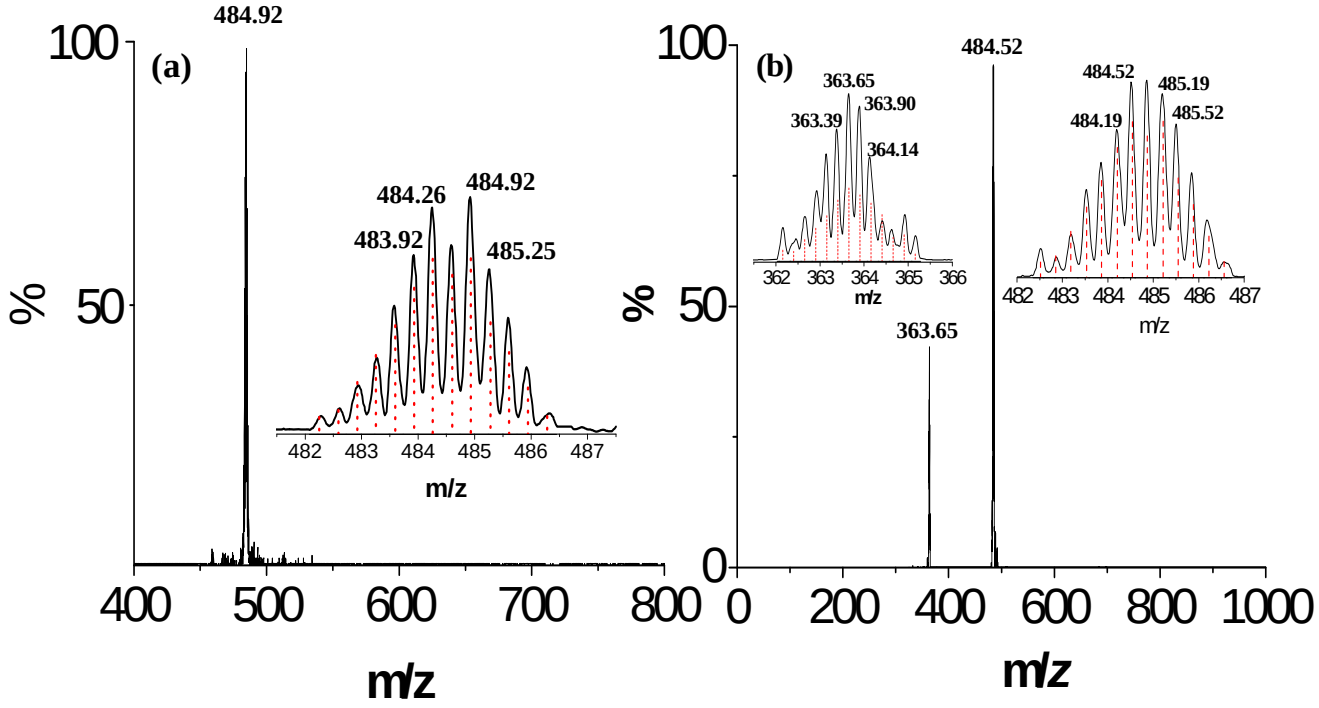

Fig. S3 ESI-MS (positive) for the complex cations, (a) $[(bpy)_2Ru(phen\text{-}bzim\text{-}tpy)Os(tpy–PhCH_3)]^{3+}$ (*m/z* = 484.92) (b) $[(bpy)_2Os(phen\text{-}Hbzim\text{-}tpy)Ru(tpy–PhCH_3)]^{4+}$ (*m/z* = 365.65) and $[(bpy)_2Os(phen\text{-}bzim\text{-}tpy)Ru(tpy–PhCH_3))]^{3+}$ (*m/z* = 484.52) in acetonitrile showing the observed and isotopic distribution patterns.

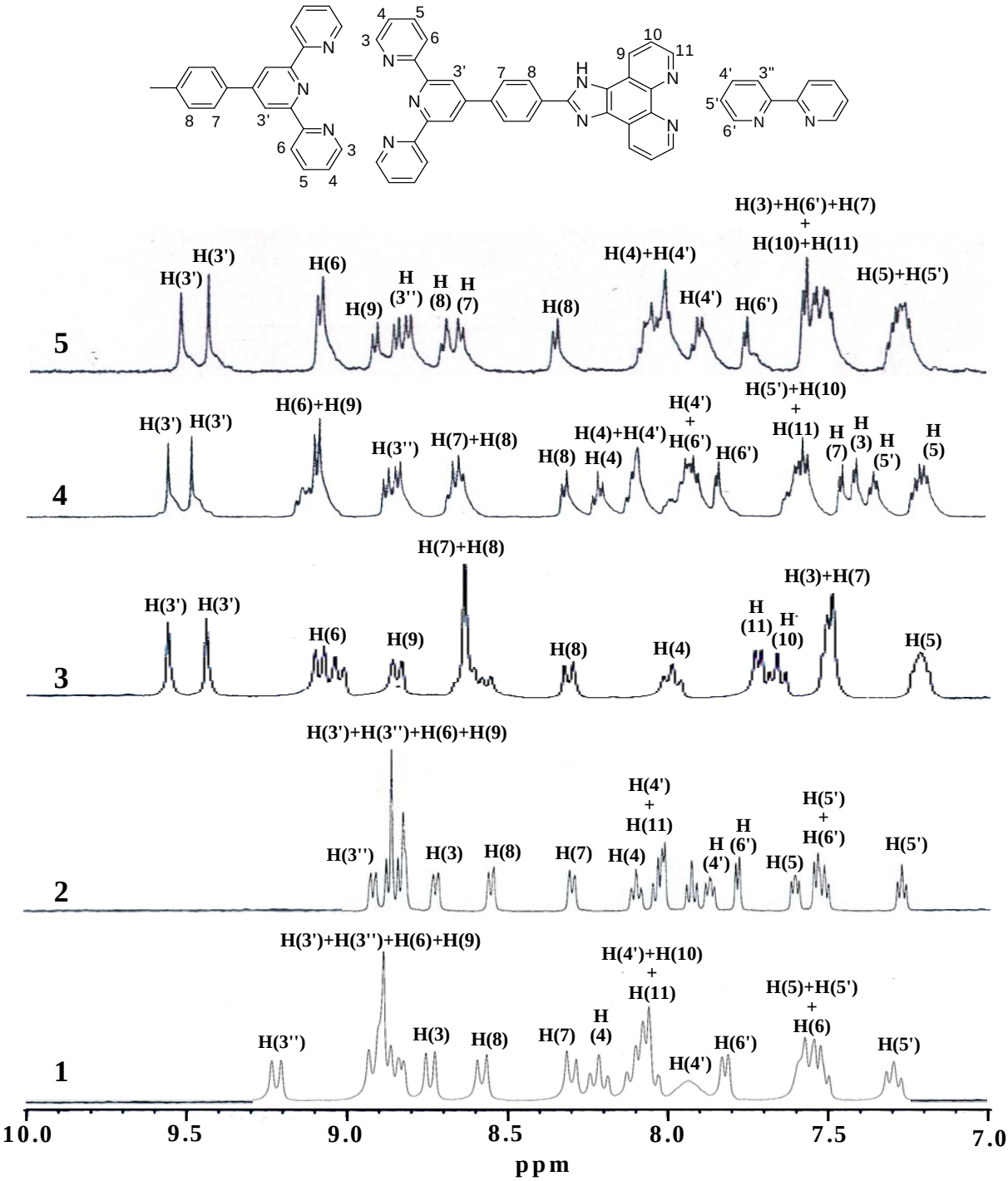

Fig. S4 ^{1}H NMR spectra of **1–5** in DMSO-d_6 at room temperature.

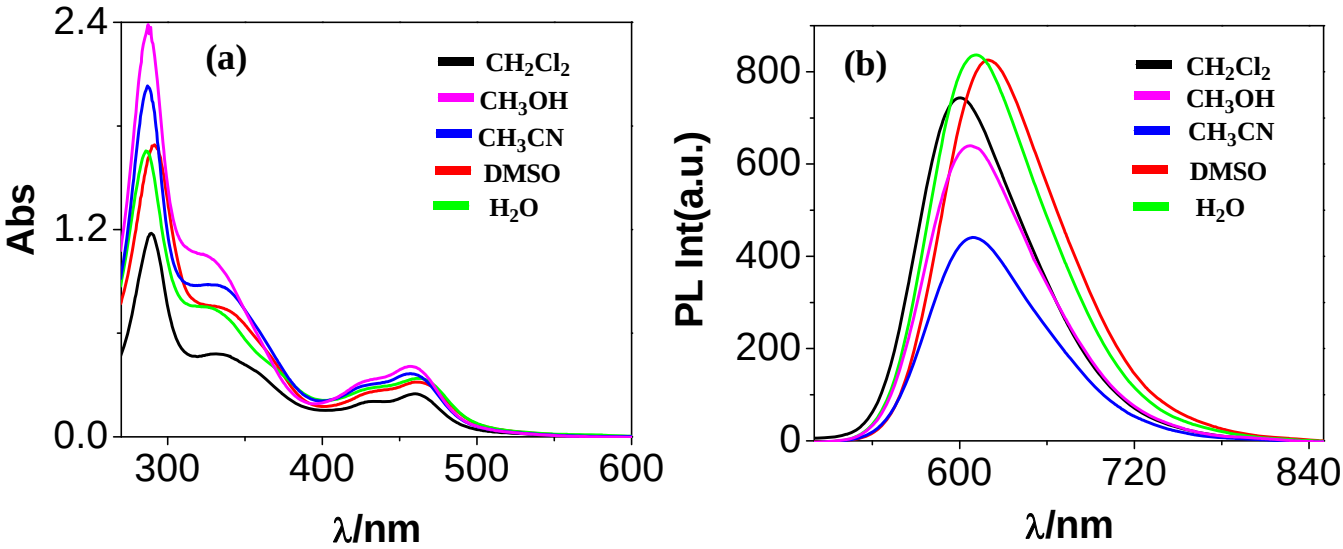

Fig. S5 (a) Absorption and (b) photoluminescence spectra of **1** in different solvents.

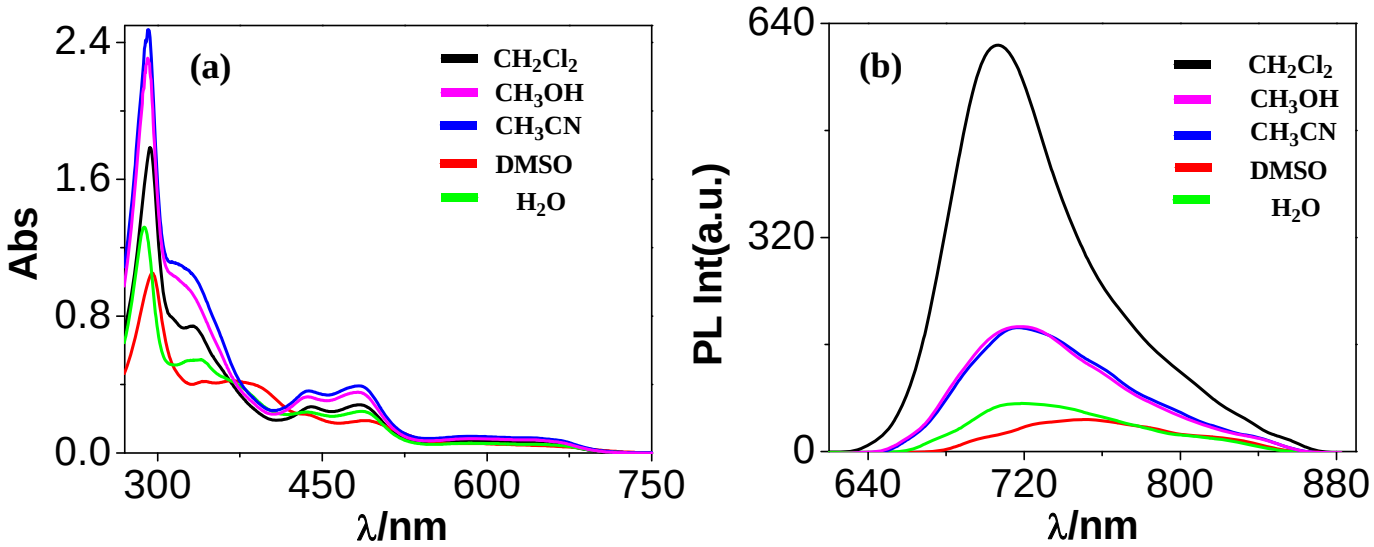

Fig. S6 (a) Absorption and (b) photoluminescence spectra of **2** in different solvents.

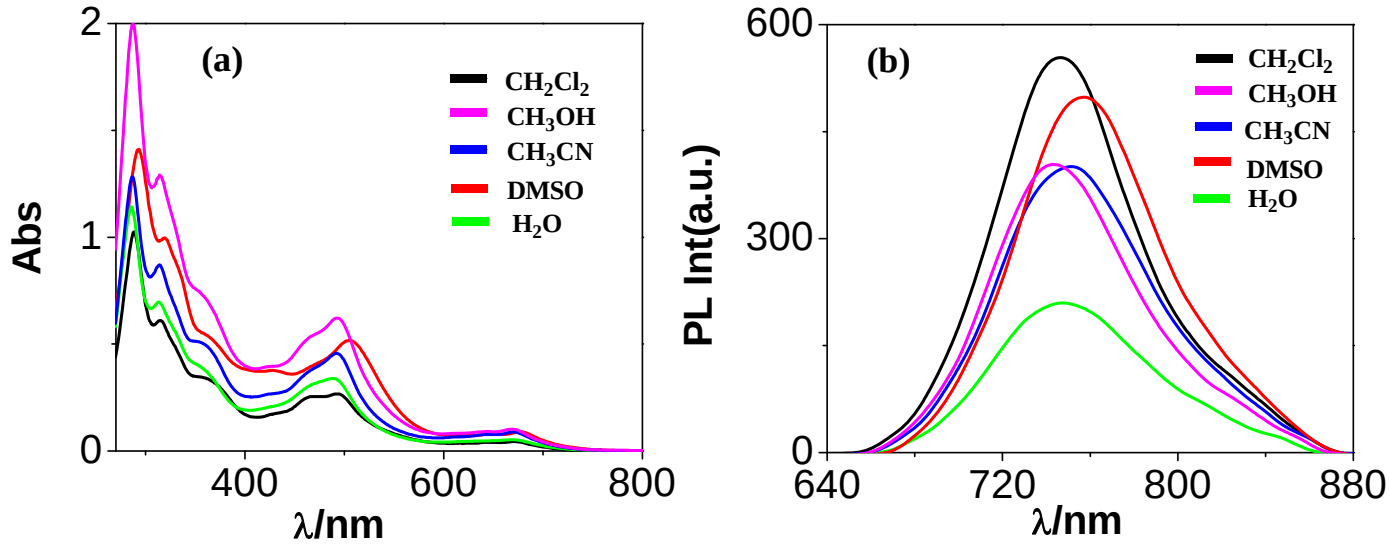

Fig. S7 (a) Absorption and (b) photoluminescence spectra of **4** in different solvents.

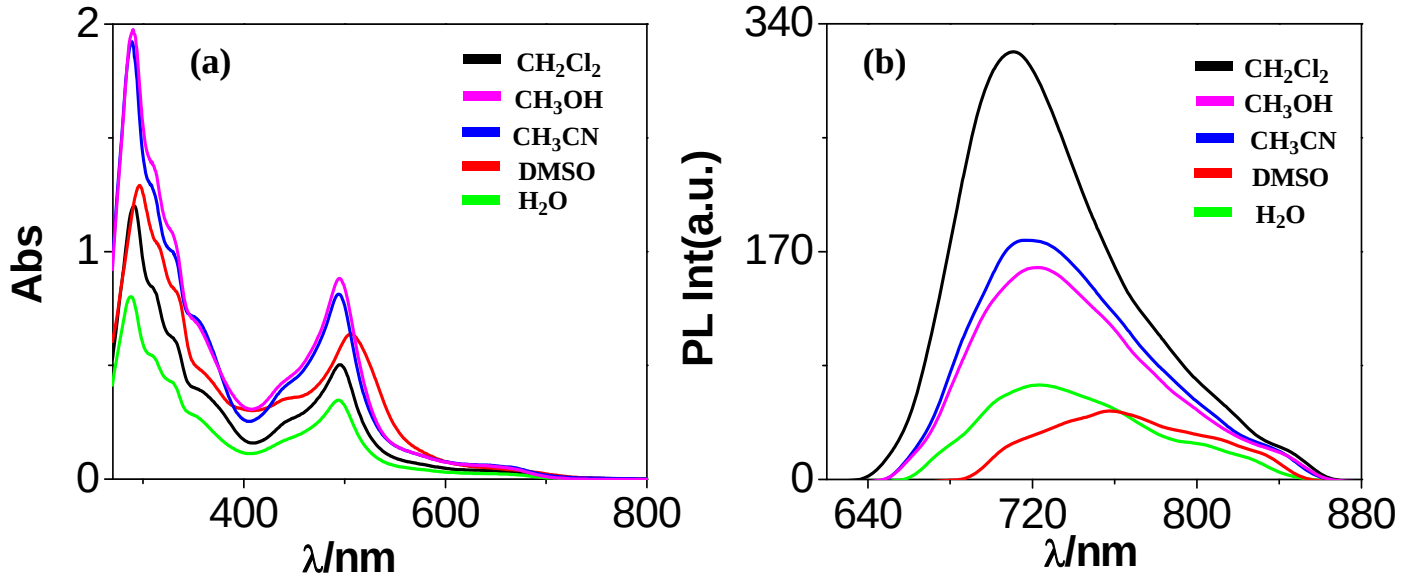

Fig. S8 (a) Absorption and (b) photoluminescence spectra of **5** in different solvents.

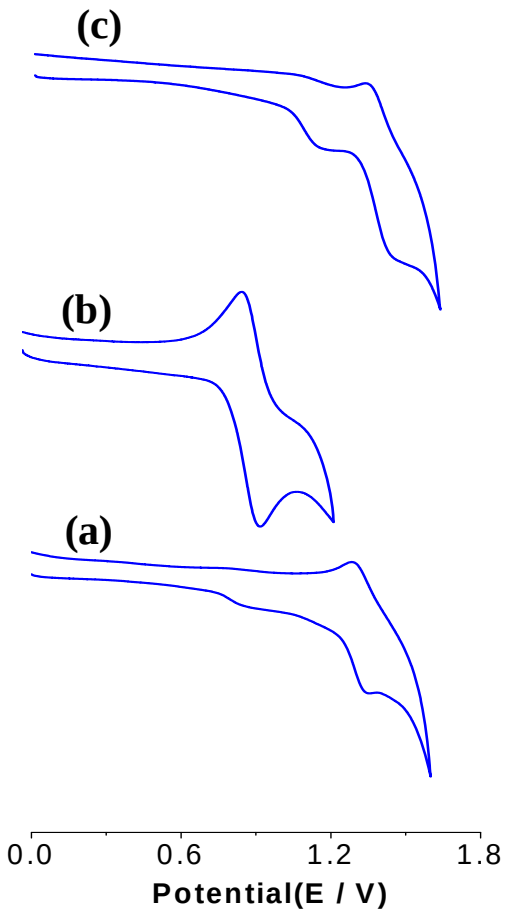

Fig. S9 Cyclic voltammograms of **1** (a), **2** (b), and **3** (c) in acetonitrile at room temperature showing the oxidation of the complexes.

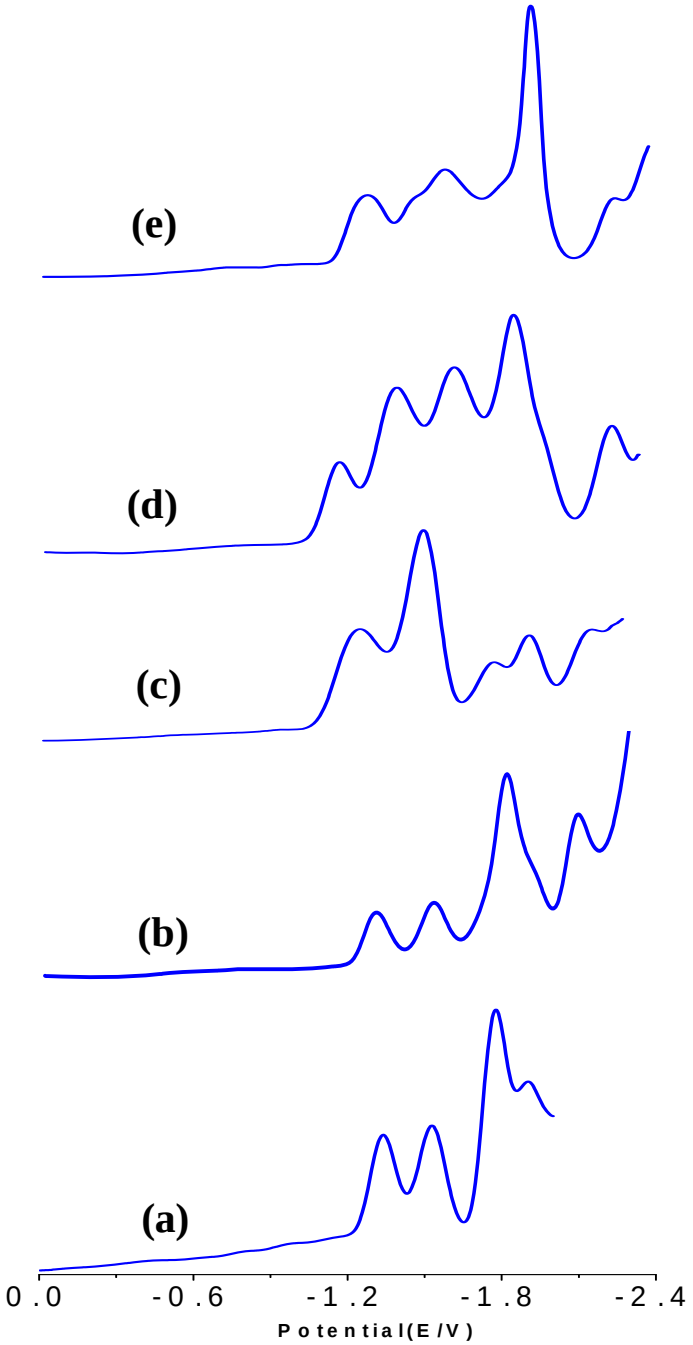

Fig. S10 Square wave voltammograms of **1** (a), **2** (b), **3** (c), **4** (d), and **5**(e) in acetonitrile at room temperature showing the reduction of the complexes.

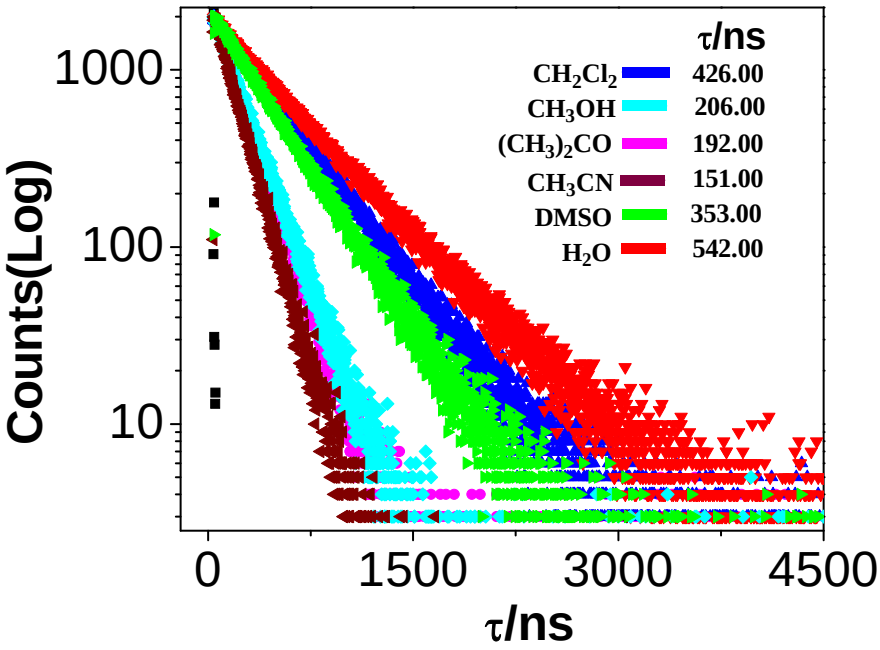

Fig. S11 Time–resolved photoluminescence decays of **1** in different solvents at room temperature. Lifetimes of the complex in different solvents are also given in the figure.

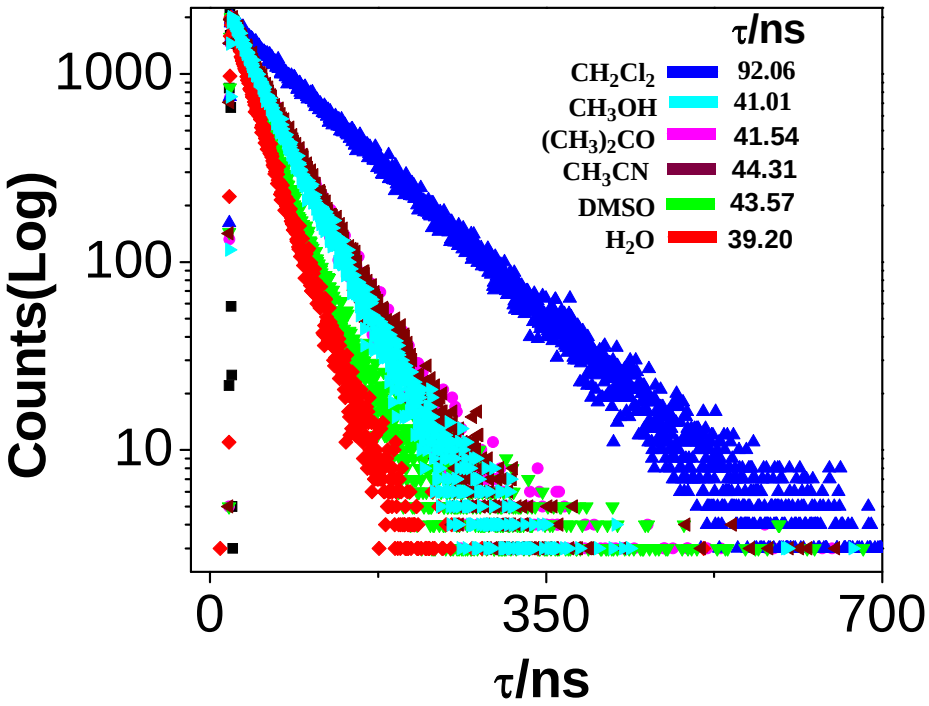

Fig. S12 Time–resolved photoluminescence decays of **2** in different solvents at room temperature. Lifetimes of the complex in different solvents are also given in the figure.

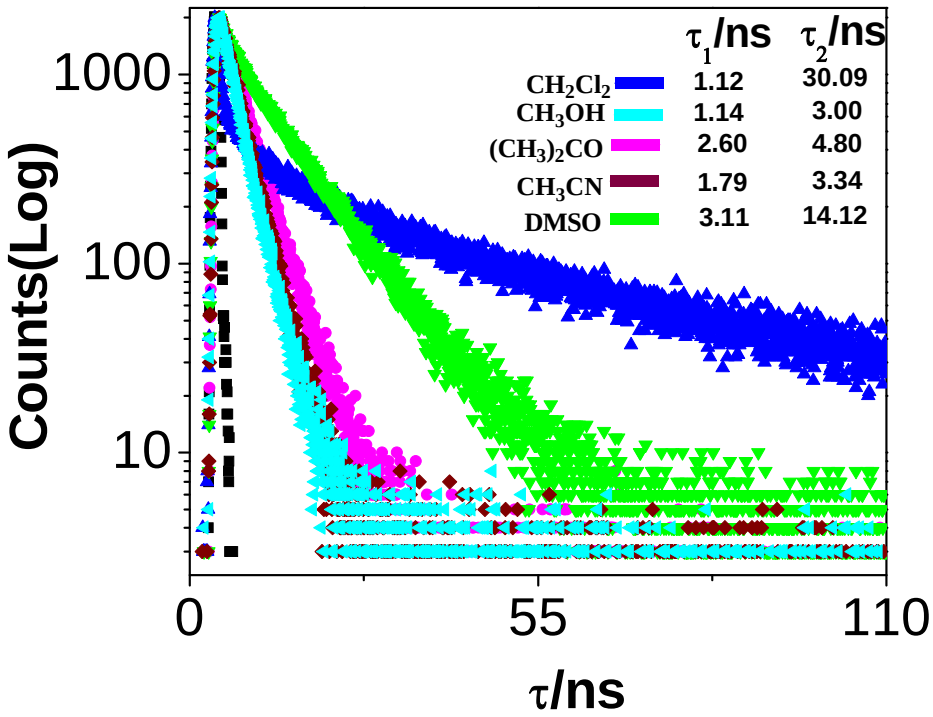

Fig. S13 Time–resolved photoluminescence decays of **3** in different solvents at room temperature. Lifetimes of the complex in different solvents are also given in the figure.

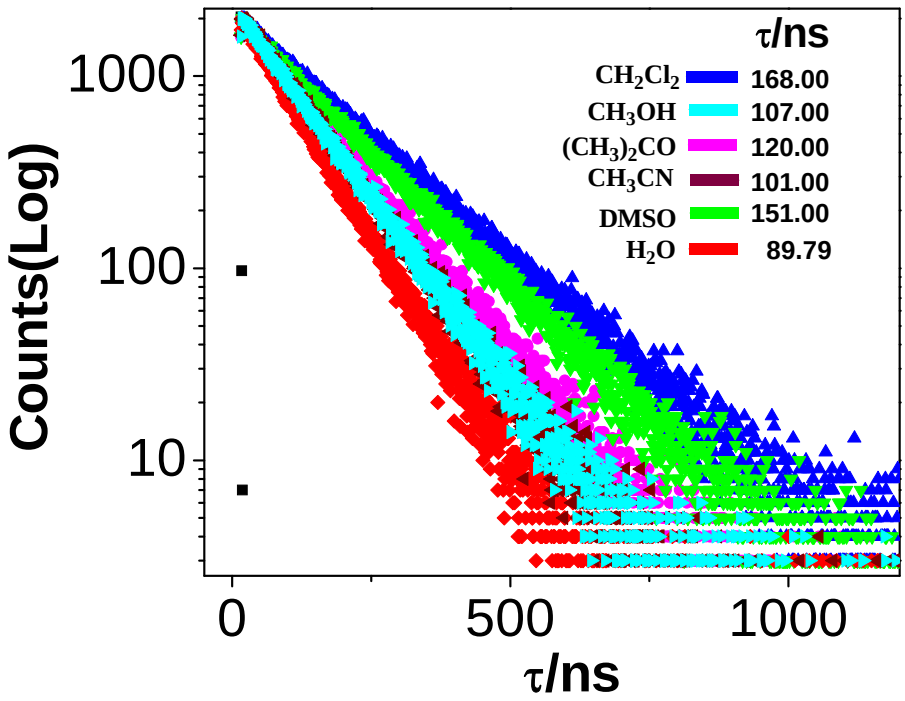

Fig. S14 Time–resolved photoluminescence decays of **4** in different solvents at room temperature. Lifetimes of the complex in different solvents are also given in the figure.

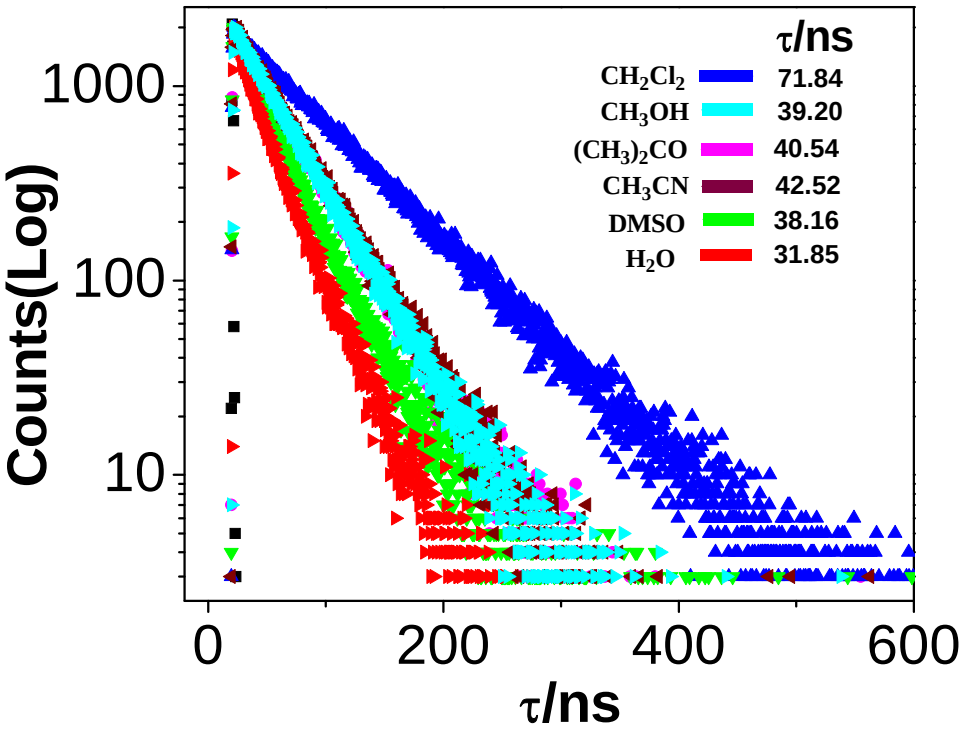

Fig. S15 Time–resolved photoluminescence decays of **5** in different solvents at room temperature. Lifetimes of the complex in different solvents are also given in the figure.

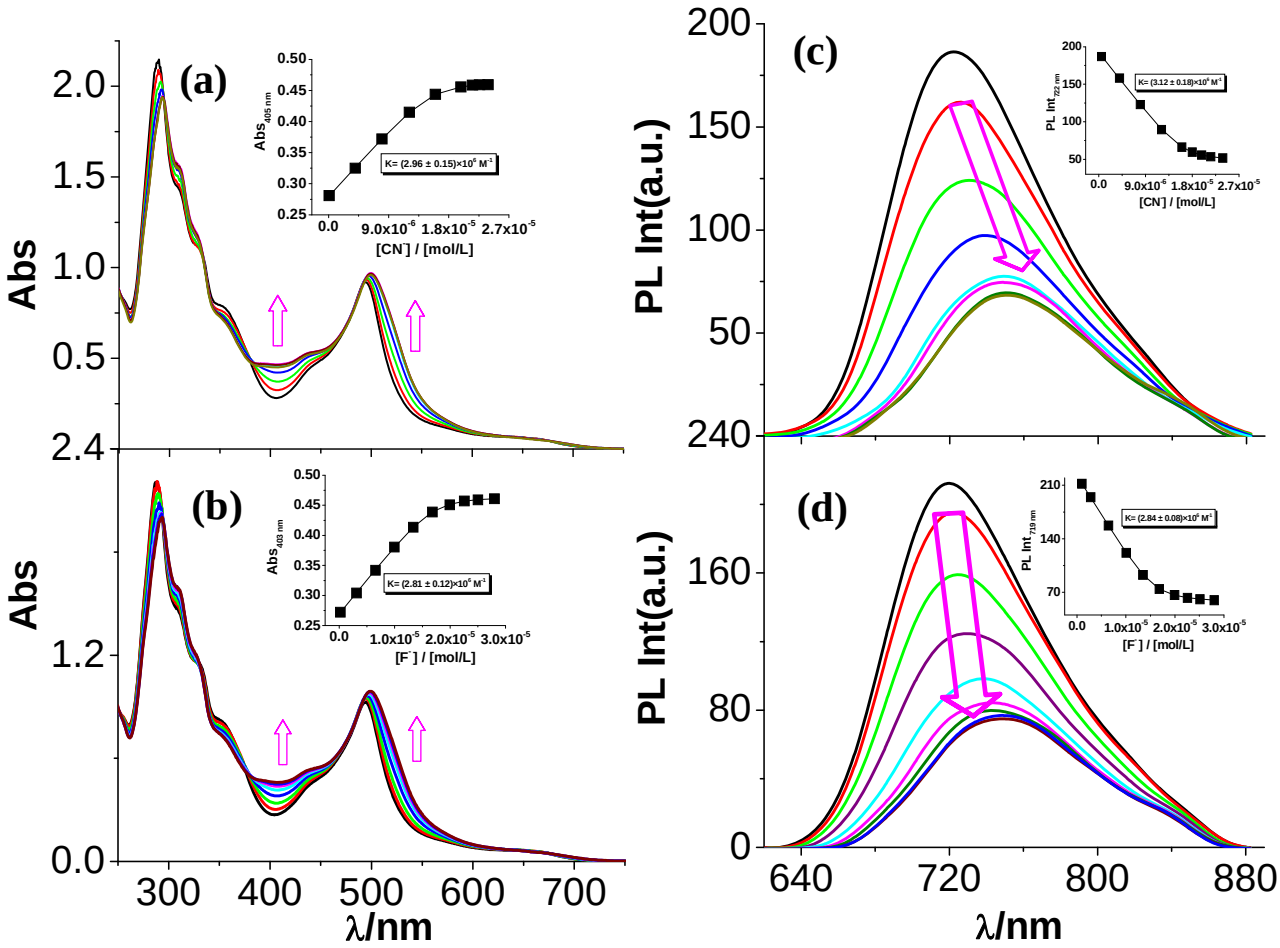

Fig. S16 Changes in UV–vis absorption and luminescence spectra of **5** in acetonitrile solution (2.0×10^{-5} M) upon incremental addition of CN^- (a and c, respectively) and F^- (b and d, respectively) ions (5.0×10^{-3} M). The insets show the fit of the experimental absorbance (a and b) and luminescence (c and d) data to a 1:1 binding profile.

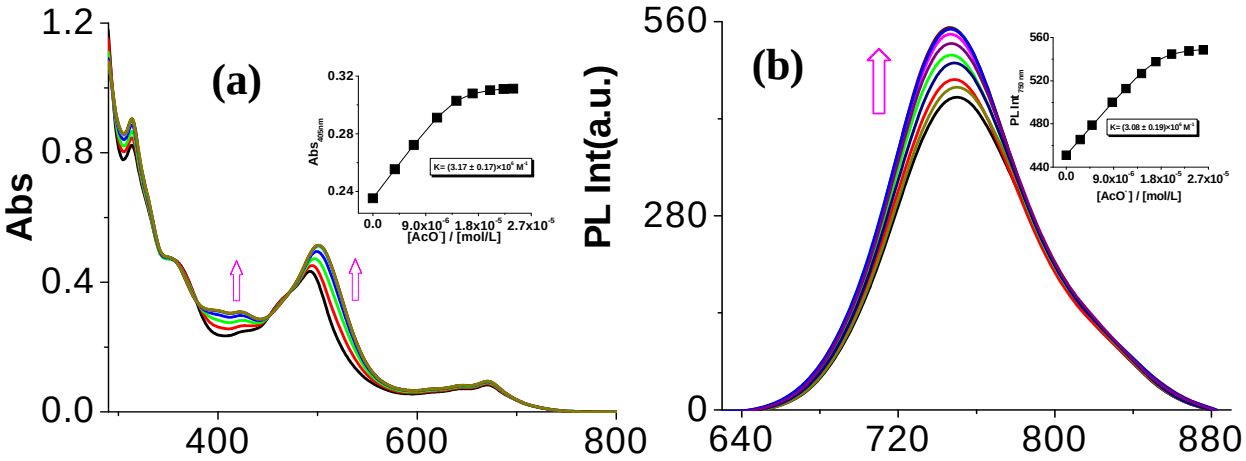

Fig. S17 Changes in UV–vis absorption and luminescence spectra of **4** in acetonitrile solution (2.0×10^{-5} M) upon incremental addition of AcO^- ion (5.0×10^{-3} M). The insets show the fit of the experimental absorbance and luminescence data to a 1:1 binding profile.

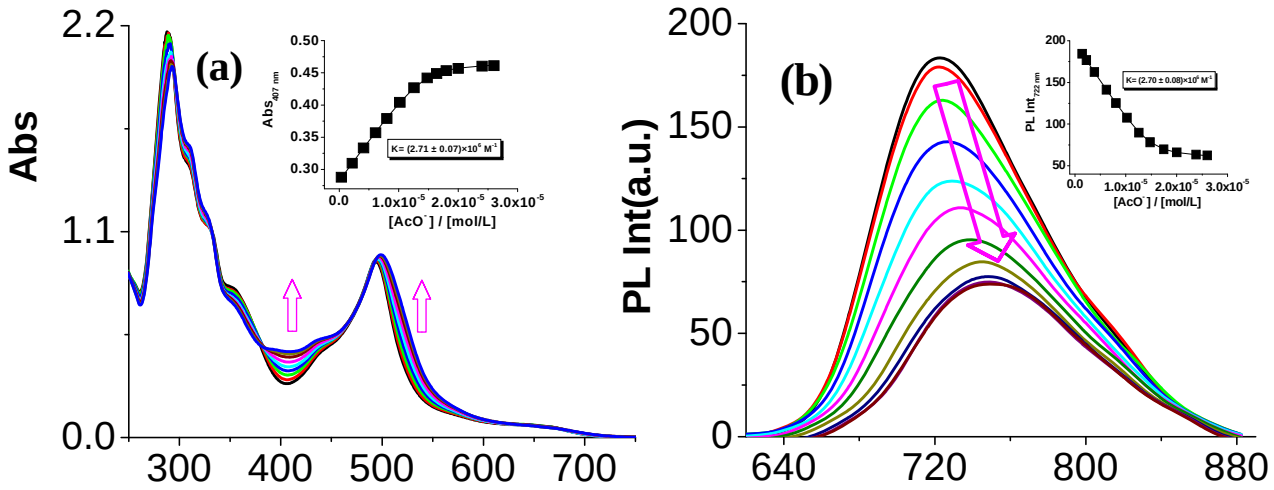

Fig. S18 Changes in UV–vis absorption and luminescence spectra of **5** in acetonitrile solution (2.0×10^{-5} M) upon incremental addition of AcO^- ion (5.0×10^{-3} M). The insets show the fit of the experimental absorbance and luminescence data to a 1:1 binding profile.

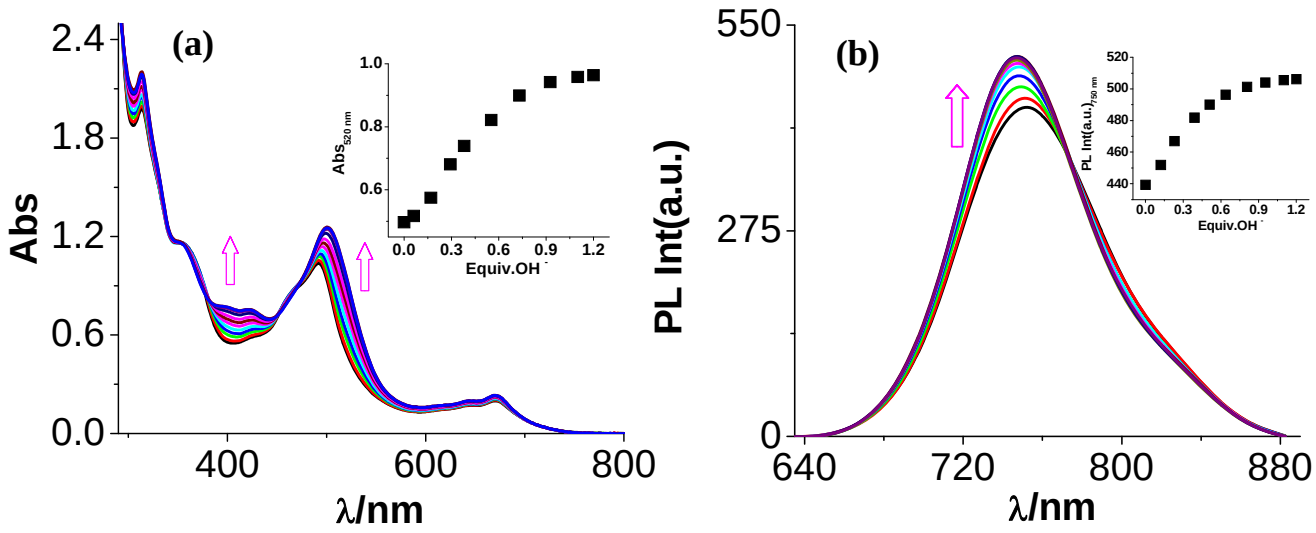

Fig. S19 Changes in UV–vis absorption and luminescence spectra of **4** in acetonitrile solution (2.0×10^{-5} M) upon incremental addition of OH^- ion (5.0×10^{-3} M). The insets show the change of absorbance and luminescence with equivalent of OH^- ion.

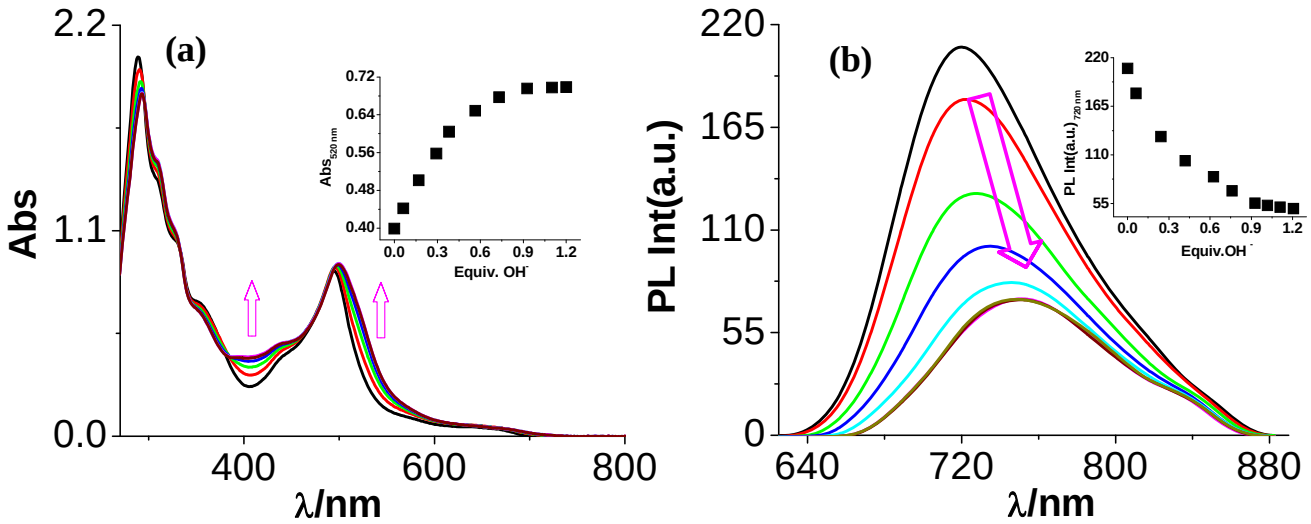

Fig. S20 Changes in UV–vis absorption and luminescence spectra of **5** in acetonitrile solution (2.0×10^{-5} M) upon incremental addition of OH^- ion (5.0×10^{-3} M). The insets show the change of absorbance and luminescence with equivalent of OH^- ion.

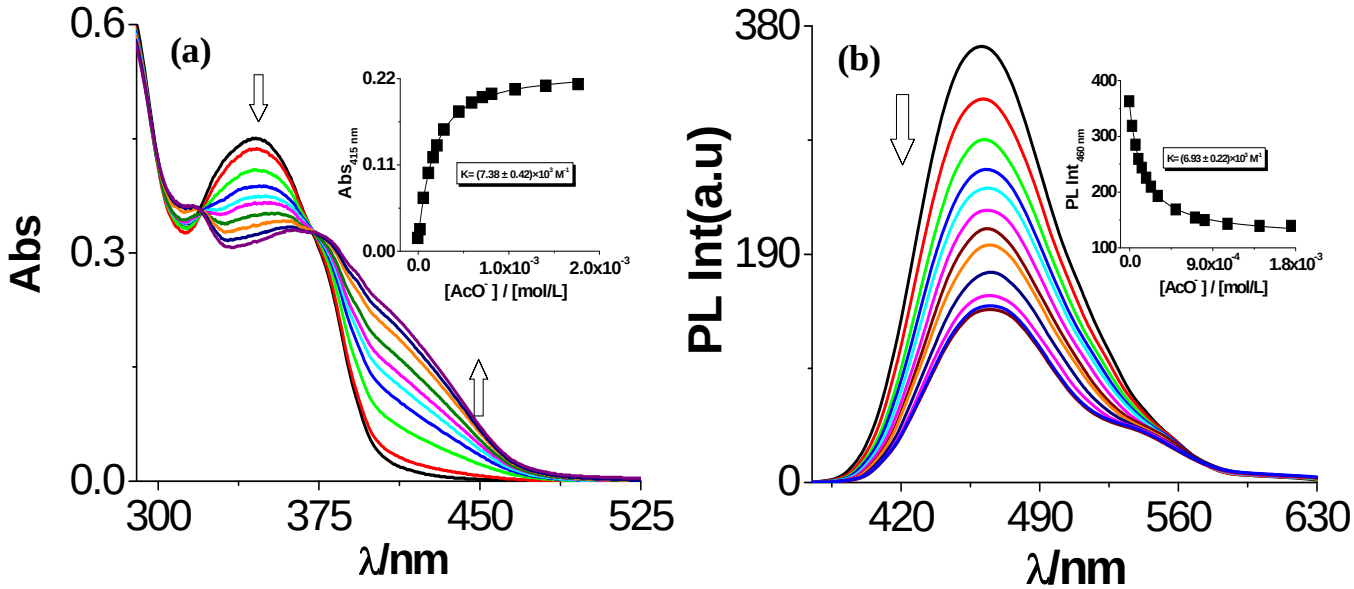

Fig. S21 Changes in UV–vis absorption (a) and luminescence (b) spectra of **phen-Hbzim-tpy** in dimethylsulfoxide solution (2.0×10^{-5} M) upon incremental addition of AcO^- ion. The insets show the fit of the experimental absorbance and luminescence data to a 1:1 binding profile.

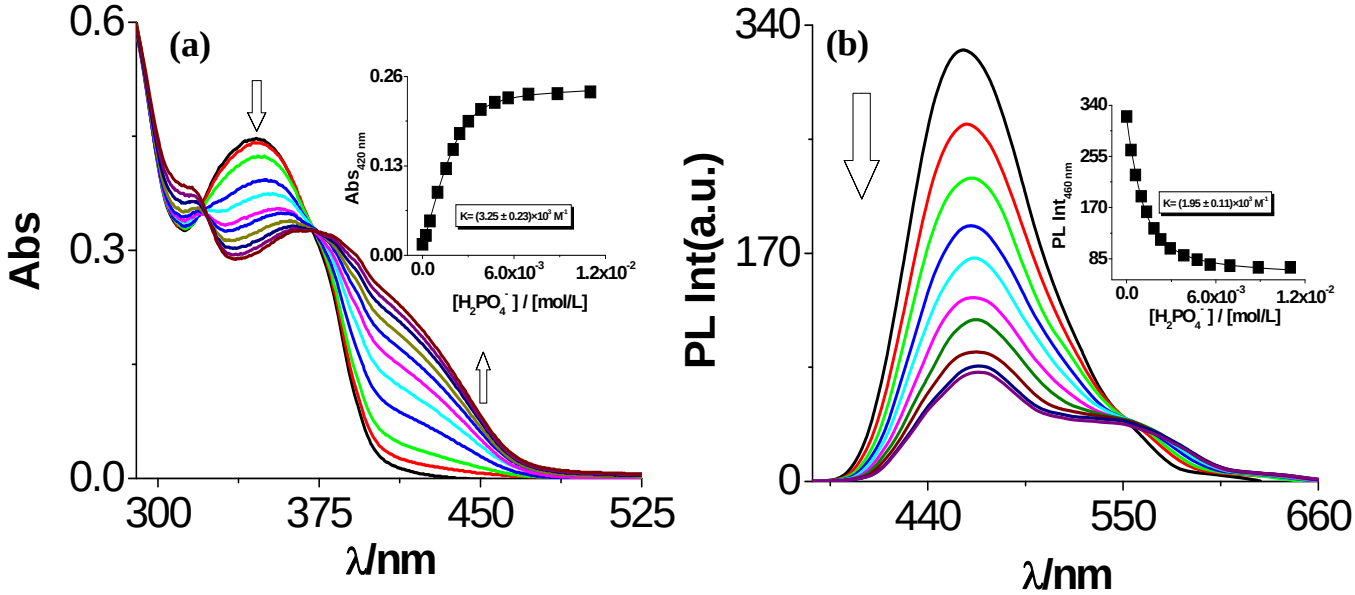

Fig. S22 Changes in UV–vis absorption (a) and luminescence (b) spectra of **phen-Hbzim-tpy** in dimethylsulfoxide solution (2.0×10^{-5} M) upon incremental addition of $H_2PO_4^-$ ion. The insets show the fit of the experimental absorbance and luminescence data to a 1:1 binding profile.

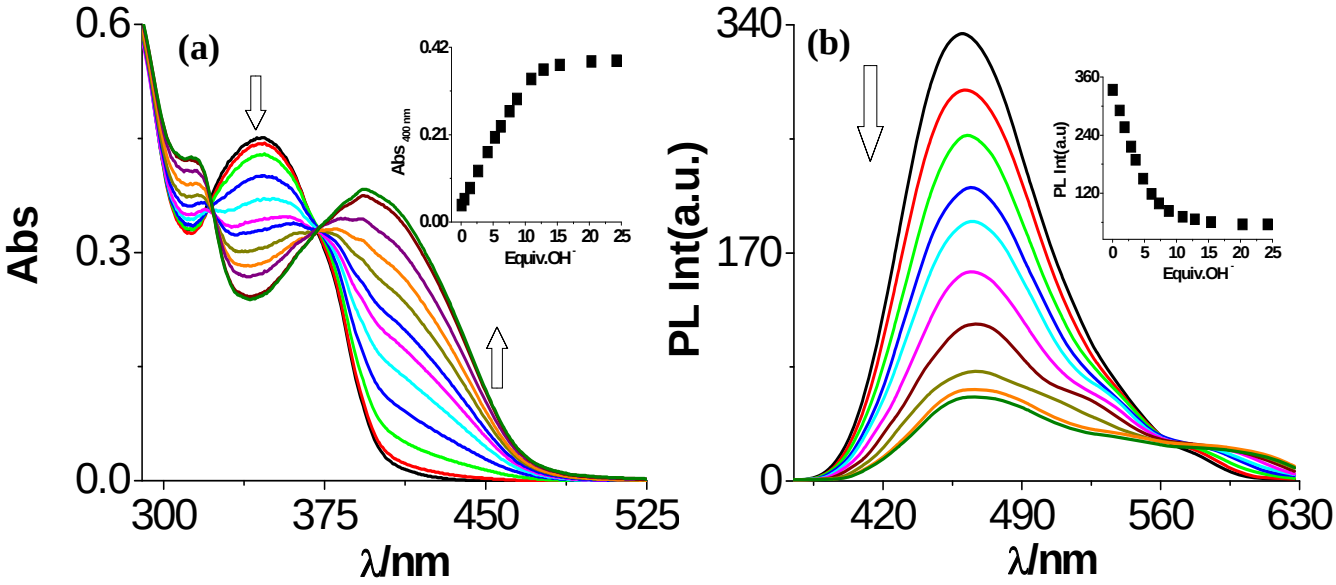

Fig. S23 Changes in UV–vis absorption and luminescence spectra of **phen-Hbzim-tpy** in acetonitrile solution (2.0×10^{-5} M) upon incremental addition of OH^- ion. The insets show the change of absorbance and luminescence with equivalent of OH^- ion.

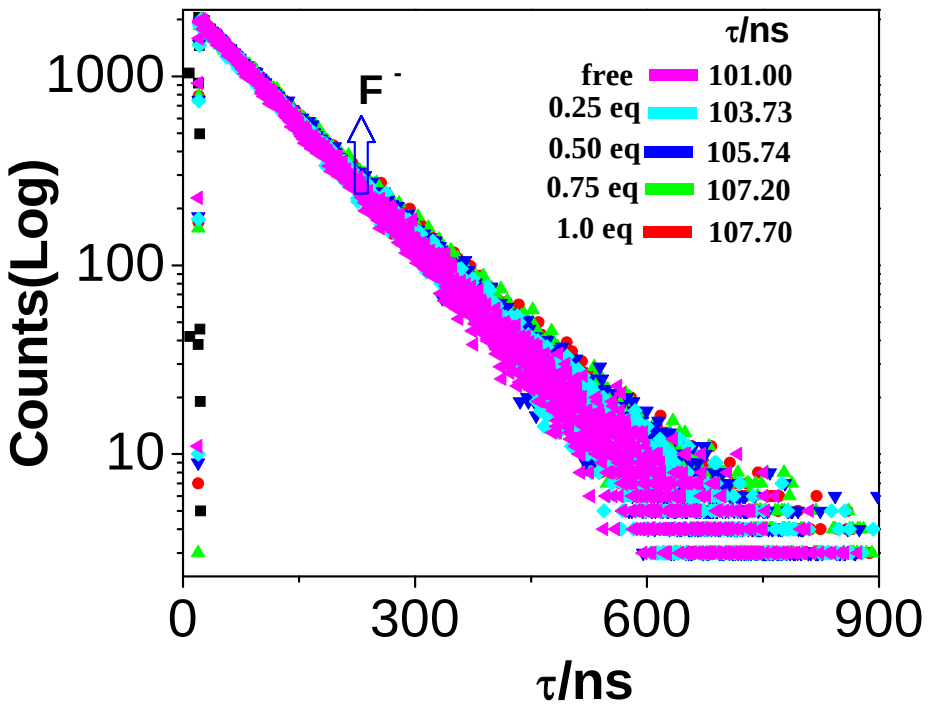

Fig. S24 Change in time-resolved luminescence decay of **4** in acetonitrile (2.0 × 10−5 M) at room temperature upon incremental addition of F^- ion (5.0 × 10−3 M). Insets show the lifetimes of the complex.

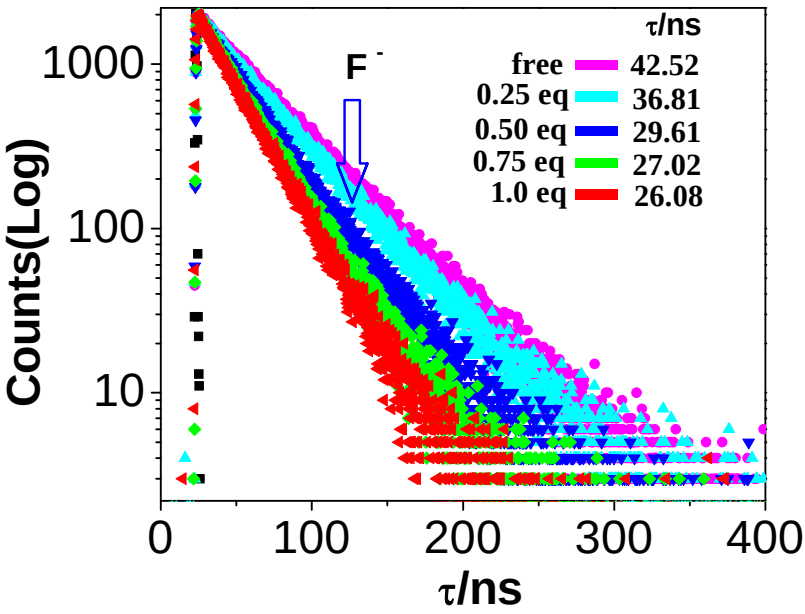

Fig. S25 Change in time-resolved luminescence decay of **5** in acetonitrile solution (2.0 × 10−5 M) at room temperature upon incremental addition of F− ion (5.0 × 10−3 M). Insets show the lifetimes of the complex.

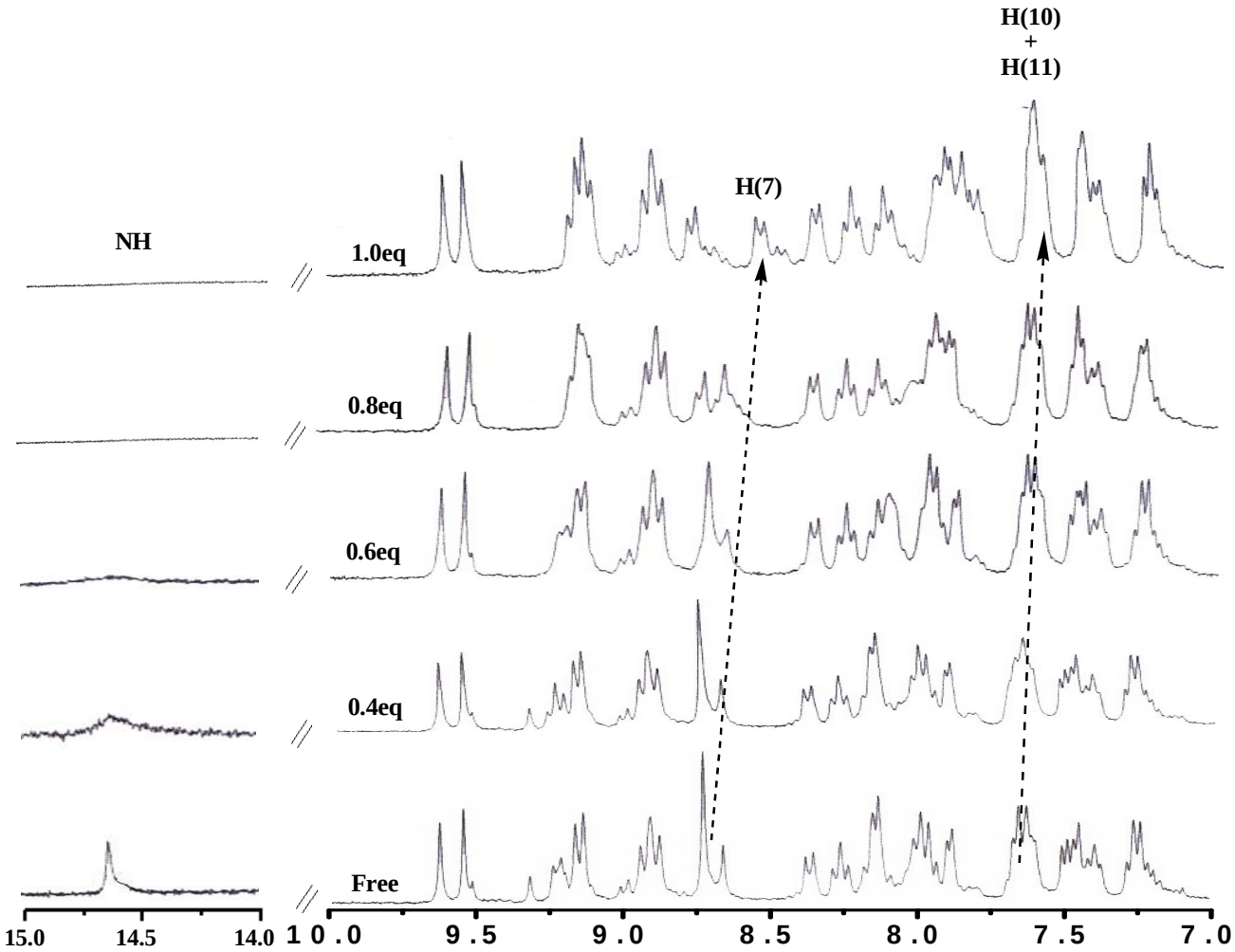

Fig. S26 ^{1}H NMR titration of sensor **4** in DMSO-d_6 solution (5.0×10^{-3} M) upon addition of F^- ion (1.25×10^{-1} M, 0–1 equivalents).

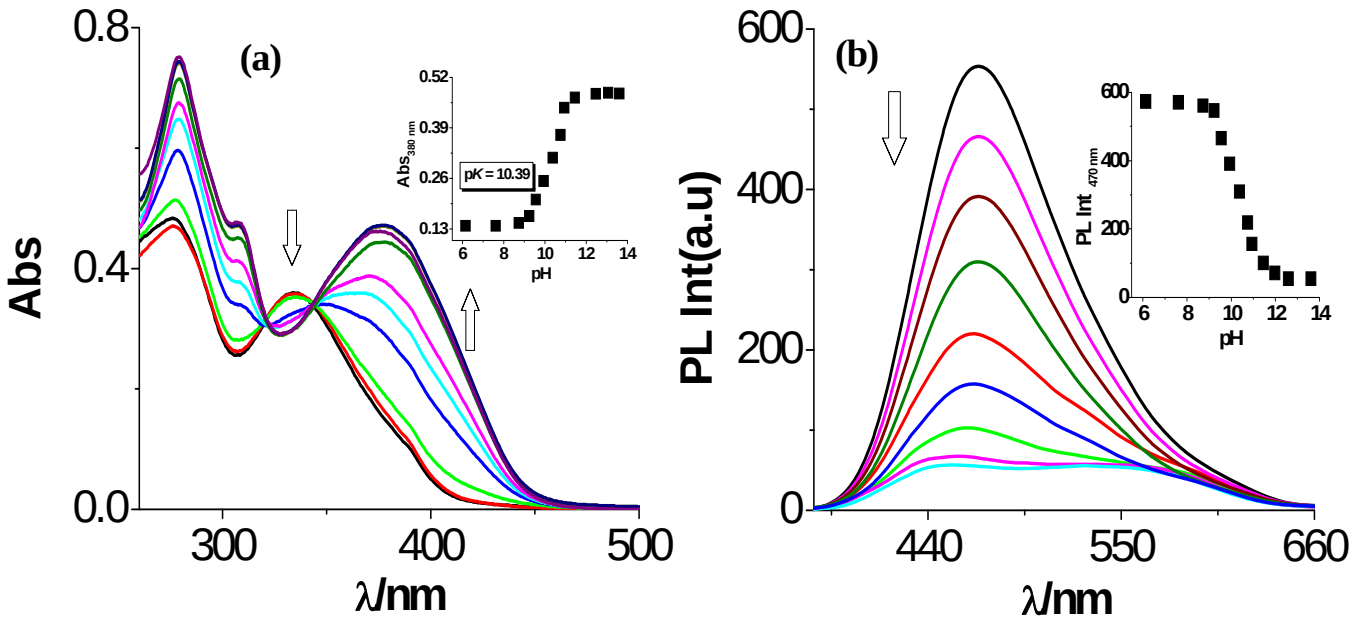

Fig. S27 Changes in UV–vis absorption (a) and luminescence (b) spectra of **phen-Hbzim-tpy** with variation of pH in dimethylsulfoxide-water (3:2 v/v). The insets show the changes of absorbance and luminescence intensities with the variation of pH.

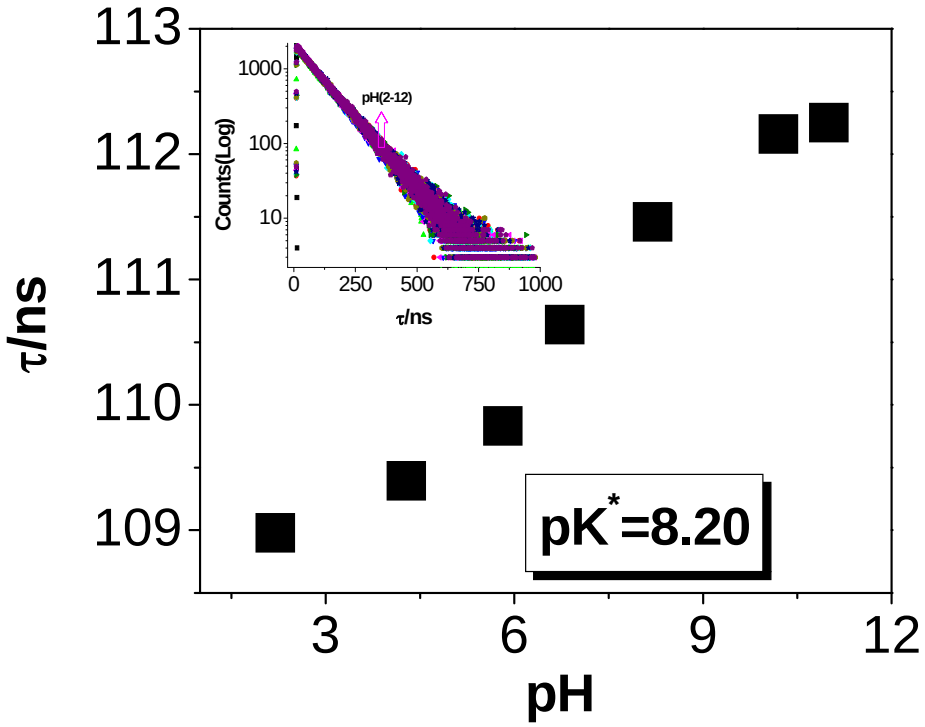

Fig. S28 Change of the luminescence lifetimes of **4** with variation of pH in acetonitrile-water (3:2 v/v). Inset shows the decay profiles of **4** as a function of pH. Excited state p*K** is also given in figure.

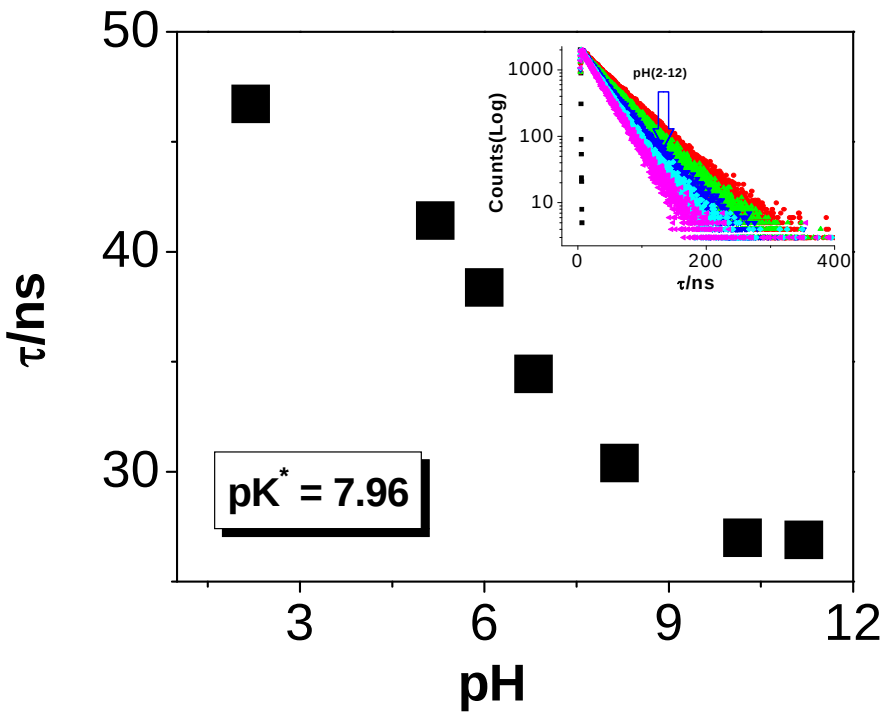

Fig. S29 Change of the luminescence lifetimes of **5** with variation of pH in acetonitrile-water (3:2). Inset shows the decay profiles of **5** as a function of pH. Excited state p*K** is also given in figure.

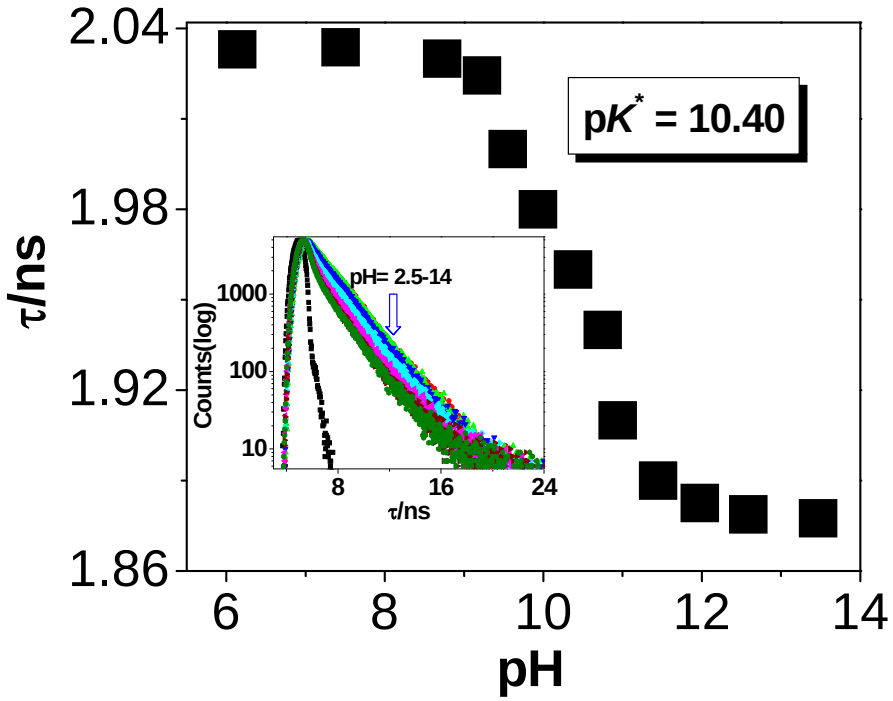

Fig. S30 Change of the luminescence lifetimes of **phen-Hbzim-tpy** with variation of pH in dimethylsulfoxide -water (3:2). Inset shows the decay profiles of **phen-Hbzim-tpy** as a function of pH. Excited state p*K** is also given in figure.